https://doi.org/10.5194/essd-2020-197
Preprint. Discussion started: 11 August 2020

Open Access Earth System Science Data Discussions

Global dataset of thermohaline staircases obtained from Argo floats and Ice Tethered Profilers

Carine G. van der Boog[1], J. Otto Koetsier[1], Henk A. Dijkstra[2], Julie D. Pietrzak[1], and Caroline A. Katsman[1]

[1]Environmental Fluid Mechanics, Civil Engineering and Geosciences, Delft University of Technology, Delft, the Netherlands
[2]Institute for Marine and Atmospheric research Utrecht, Utrecht University, Utrecht, the Netherlands

Correspondence: Carine van der Boog (c.g.vanderboog@tudelft.nl)

Abstract. Thermohaline staircases arise from double diffusive processes. They are characterised by stepped structures consisting of mixed layers of typically tens of meters thick that are separated by much thinner gradient layers. Through these gradient layers enhanced diapycnal salt and heat transport take place. In this study, we present a global dataset of thermohaline staircases derived from observations of Argo profiling floats and Ice Tethered Profilers using a novel detection algorithm. To establish the presence of stepped thermohaline staircases, the algorithm detects subsurface mixed layers and analyses the gradient layers in between. Of each detected staircase, the temperature, salinity, depth and height, as well as some other properties of the mixed layers and gradient layers are computed. The algorithm is applied to 487,647 quality-controlled temperature and salinity profiles to obtain the global dataset. The performance of the algorithm is verified through an analysis of independent regional observations. The algorithm and global dataset are available at the 4TU centre for research data (van der Boog et al. (2020), doi: https://doi.org/10.4121/uuid:f6529d31-b285-46ac-990b-5f45839f4e11)

1 Introduction

Thermohaline staircases consist of subsurface mixed layers that are separated by gradient layers. They arise from double diffusive processes, which in turn result from a two orders in magnitude difference between the molecular diffusivity of heat and that of salt (Stern, 1960). Whenever the vertical gradients of temperature- and salinity-induced stratification have the same sign, these differences in molecular diffusivity can enhance the vertical mixing through double diffusive convection, leading to effective diffusivities in the order of 10^{-4} m^{-2} s^{-1} and the formation of thermohaline staircases (Radko, 2013, and references therein).

Based on the the Turner angle (Tu), which compares the density component of the temperature distribution with the density component of the salinity distribution, two regimes of double diffusion can be distinguished (Ruddick, 1983). Waters with $-90° < Tu < -45°$ correspond to a stratification where both temperature and salinity increase with depth and belong to the

https://doi.org/10.5194/essd-2020-197
Preprint. Discussion started: 11 August 2020

Open Access Earth System Science Data Discussions

diffusive-convective regime. Those with $45° < Tu < 90°$ correspond to a stratification where temperature and salinity decrease with depth and belong to the salt-finger regime.

Theoretical and laboratory studies have indicated that diapycnal fluxes of heat and salt in thermohaline staircases are elevated compared to the background turbulence (e.g., Schmitt, 1981; Kelley, 1990; Radko and Smith, 2012; Garaud, 2018). These results were confirmed by a tracer release experiment in the western tropical Atlantic Ocean (Schmitt et al., 2005). Although these enhanced fluxes were observed, the importance of these fluxes for the global mechanical energy budget remain unknown.

Besides the enhanced mixing, the vertical heat and salt fluxes in thermohaline staircases can affect water mass properties. In some regions, persistent thermohaline staircases with layers stretching horizontally over a few hundred kilometers have been observed (Schmitt et al., 1987; Timmermans et al., 2008; Shibley et al., 2017), which results in significant diapycnal fluxes between water masses. For example, the double diffusive diapycnal fluxes in the Mediterranean Sea dominate the transport between the deep water masses (Zodiatis and Gasparini, 1996; Bryden et al., 2014; Schroeder et al., 2016), and in the Arctic Ocean and Southern Ocean, double diffusion regulates sea-ice formation (Timmermans et al., 2008; Shibley et al., 2017; Polyakov et al., 2012; Bebieva and Timmermans, 2019).

Modelling studies that incorporated parameterizations of double diffusive fluxes, indicated that the associated double-diffusive diapycnal fluxes have global implications (Gargett and Holloway, 1992; Merryfield et al., 1999; Oschlies et al., 2003). To study these implications, we present here a global dataset of the occurrence of thermohaline staircases and their properties. The dataset is based on observations from Argo floats and Ice Tethered Profilers. In the following sections we briefly describe the raw data used to extract the dataset (Section 2) and the algorithm we designed to detect staircase structures (Section 3). The sensitivity of this detection algorithm to the chosen input parameters is assessed in Section 4. The dataset is verified in Section 5, followed by some guidelines for the use of the dataset in Section 6.

2 Data pre-processing

The dataset contains observations of autonomous Argo floats and autonomous Ice Tethered Profilers (ITP). The data of all active and inactive profilers is obtained from http://www.argo.ucsd.edu and http://www.whoi.edu/itp (on 14 May 2020). Details on the profilers are described in Krishfield et al. (2008) and Toole et al. (2011) for the ITP and in Argo (2000) for the Argo floats. First a quality check is performed to ensure the quality of the temperature and salinity profiles analysed. A profile is excluded from analysis if it was taken by an Argo float mentioned on the grey list. As thermohaline staircases consist of mixed layers with depths of tens of meters, we also require that profiles have continuous data up to 500 dbar with an average resolution finer than 5 dbar. After this quality control, 487,647 vertical temperature and salinity profiles remain. Their global distribution is shown in Figure 1.

Next, all profiles are linearly interpolated to a vertical resolution of 1 dbar from the surface to 2000 dbar. From these interpolated profiles we calculate several variables. Absolute salinity (S) in g kg^{-1} and conservative temperature (T) in °C are computed with the TEOS-10 software (McDougall and Barker, 2011). We applied a moving average of 200 dbar (Table 1) to obtain the background temperature and salinity profiles of the water column ($\bar{T}$ and $\bar{S}$, respectively) and to compute the

https://doi.org/10.5194/essd-2020-197
Preprint. Discussion started: 11 August 2020

Open Access Earth System Science Data Discussions

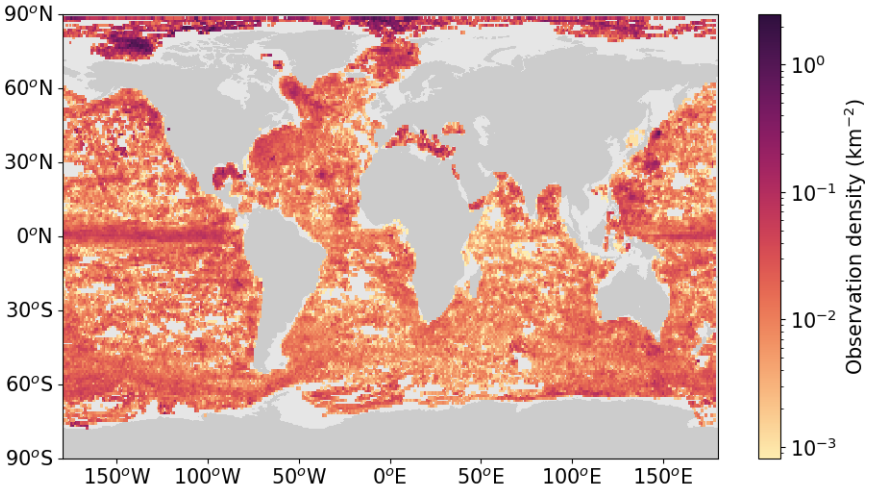

Figure 1. Observation density of the number of profiles obtained from the Argo floats and Ice Tethered Profilers after quality control (in km^{-2}). Observation density is binned per degree longitude and degree latitude. Empty bins indicate that no data was available at that location.

Table 1. Input parameters applied during the data pre-processing and the algorithm as used in this study. The sensitivity of the output of the algorithm to the input variables is discussed in the Section 4.

parameter	description	value
moving average window	chosen to obtain background profiles	200 dbar
$\partial\sigma_1/\partial p_{max}$	density gradient threshold for detection mixed layer	0.0005 kg m^{-3} dbar^{-1}
$\Delta\sigma_{1,ML,max}$	maximum density gradient within mixed layer	0.005 kg m^{-3}
$h_{GL,max}$	maximum gradient layer height	30 dbar

thermal expansion coefficient (α in °C^{-1}) and the haline contraction coefficient (β in kg g^{-1}). A consequence of the moving average of 200 dbar is that the upper 100 dbar and lower 100 dbar of each profile is omitted in the remainder of the analysis. The Turner angle is computed using smoothed profiles with a moving average of 50 dbar, which is similar to Shibley et al. (2017), following Ruddick (1983), from

$$Tu = \tan^{-1}\left(\alpha\frac{\partial\overline{T}}{\partial p} - \beta\frac{\partial\overline{S}}{\partial p}, \alpha\frac{\partial\overline{T}}{\partial p} + \beta\frac{\partial\overline{S}}{\partial p}\right), \quad (1)$$

where the vertical gradients are approximated with a central differences scheme.

https://doi.org/10.5194/essd-2020-197
Preprint. Discussion started: 11 August 2020

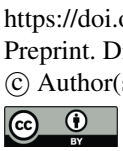

Open Access Earth System Science Data Discussions

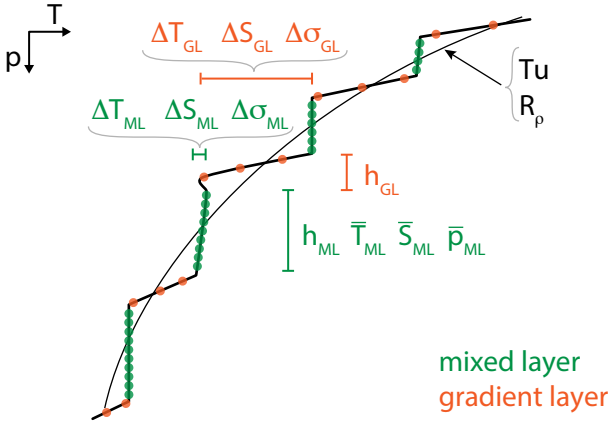

Figure 2. Schematic of a typical temperature profile with staircases, indicating the definitions of the quantities used to detect the thermohaline staircases (green: mixed layer; orange: gradient layer).

3 Detection algorithm

After the data pre-processing, we apply a detection algorithm that exploits the vertical structure of staircase profiles (Fig. 2). The detection algorithm consists of five steps. First the algorithm detects all data points that are located in the subsurface mixed layers (ML, green dots in Fig. 2) by identifying weak vertical density gradients in T and S. Next, the layer between these mixed layers (the gradient layers, GL, orange dots in Fig. 2) is assessed by applying a minimum temperature and salinity variations. Third, the height of the gradient layer and variations within the gradient layer are limited. The fourth step determines the regime of double diffusion (diffusive convection or salt fingers), and the fifth step is the identification of sequences of gradient layers, which eventually characterises the thermohaline staircases. In the following subsections, each algorithm step is described in more detail.

3.1 Mixed layers

The first step of the detection algorithm is the identification of the mixed layers. Preferably, this is done by assessing a density difference relative to a reference pressure, which is the most reliable method to detect a mixed layer (Holte et al., 2017). However, in the case of a thermohaline staircase it is necessary to detect subsurface mixed layers where the reference pressure is unknown beforehand. To determine this reference pressure, a threshold gradient criterium is applied first (Dong et al., 2008). In this criterium, vertical density gradients are identified as a mixed layer whenever the gradients are below a certain threshold.

We apply the gradient criterium on the vertical gradients of the potential density anomaly at a reference pressure of 1000 dbar (σ_1). We used a threshold of $\partial\sigma_1/\partial p_{max}$ =0.0005 kg m^{-3} dbar^{-1} (Table 1), which is similar to mixed layer gradients used by Bryden et al. (2014). Furthermore, this threshold gradient is well above the threshold used by Timmermans et al. (2008), who used 0.005°C m^{-1} (which corresponds to $\partial\sigma_1/\partial p_{max}$ =0.00036 kg m^{-3} dbar^{-1}). The threshold gradient method

https://doi.org/10.5194/essd-2020-197
Preprint. Discussion started: 11 August 2020

Open Access Earth System Science Data Discussions

is applied on both temperature and salinity profiles, i.e.,

$$\left|\alpha\rho_0\frac{\partial T}{\partial p}\right| \leq 0.0005 \text{ kg m}^{-3}\text{dbar}^{-1},$$
$$\left|\beta\rho_0\frac{\partial S}{\partial p}\right| \leq 0.0005 \text{ kg m}^{-3}\text{dbar}^{-1}. \quad (2)$$

Also the vertical density gradients from the combined temperature and salinity effects must satisfy this condition:

$$\left|\frac{\partial \sigma_1}{\partial p}\right| \leq 0.0005 \text{ kg m}^{-3}\text{dbar}^{-1}. \quad (3)$$

These three conditions ensure that the vertical temperature, salinity and density gradients are all below the threshold value. At each pressure level where all three conditions are met the datapoint is identified as a mixed layer. Next, for each continuous sequence of datapoints, the algorithm computes the average pressure. This is then used as a reference pressure, which is required to be able to apply the mixed layer detection.

At every reference pressure, a maximum density range is required within the mixed layers to identify the full vertical extent of each mixed layer. To allow for small variations of temperature and salinity in the mixed layer, but to exclude variations in the gradient layer, we use a threshold of $\Delta\sigma_{1,ML,max}$ =0.005 kg m^{-3} for density variations within each mixed layer (Table 1). This density range corresponds to the density range used by Holte et al. (2017) for the detection of surface mixed layers. The applied density range allows for mixed layers with heights in the order of 10 m assuming gradients of $\partial\sigma_1/\partial p_{max}$ =0.0005 kg m^{-3} dbar^{-1}. To ensure separation between individual mixed layers, the upper and lower datapoint of each mixed layer are removed. Note that this results in a minimum gradient layer height of 2 dbar. After applying the threshold for density range, the algorithm defines each continuous set of datapoints as a mixed layer and computes the average pressure ($\overline{p}_{ML}$), average temperature ($\overline{T}_{ML}$), average salinity ($\overline{S}_{ML}$), mixed layer density ratio ($\overline{R}_\rho = \alpha\frac{\partial\overline{T}}{\partial p}/\left(\beta\frac{\partial\overline{S}}{\partial p}\right)$), average Turner angle ($\overline{Tu}_{ML}$) and height (h_{ML}) for each mixed layer.

3.2 Gradient layers: temperature and salinity variations

The algorithm defines a gradient layer as the part of the water column between two mixed layers. In addition, to ensure a stepped structure the algorithm requires that the temperature, salinity and density variations within each mixed layer should be smaller than the variations in the gradient layer (Fig. 2):

$$\begin{aligned}\max\left(|\Delta T_{ML,1}|,|\Delta T_{ML,2}|\right) &< |\Delta T_{GL}|;\\ \max\left(|\Delta S_{ML,1}|,|\Delta S_{ML,2}|\right) &< |\Delta S_{GL}|;\\ \max\left(|\Delta\sigma_{1,ML,1}|,|\Delta\sigma_{1,ML,2}|\right) &< |\Delta\sigma_{1,GL}|;\end{aligned} \quad (4)$$

where the subscripts 1 and 2 correspond to the mixed layer directly above and below a gradient layer, respectively. It appears that most data points that meet these requirements (orange histograms in Fig. 3a-c) have Turner angles in the two double diffusive regimes. This dependence of the variations in the gradient layers on the Turner angle is in line with expectations that staircase-like structures are mostly found within double diffusive regimes. In total, 28 % of all detected gradient layers meet all three requirements (Fig. 3d).

https://doi.org/10.5194/essd-2020-197
Preprint. Discussion started: 11 August 2020

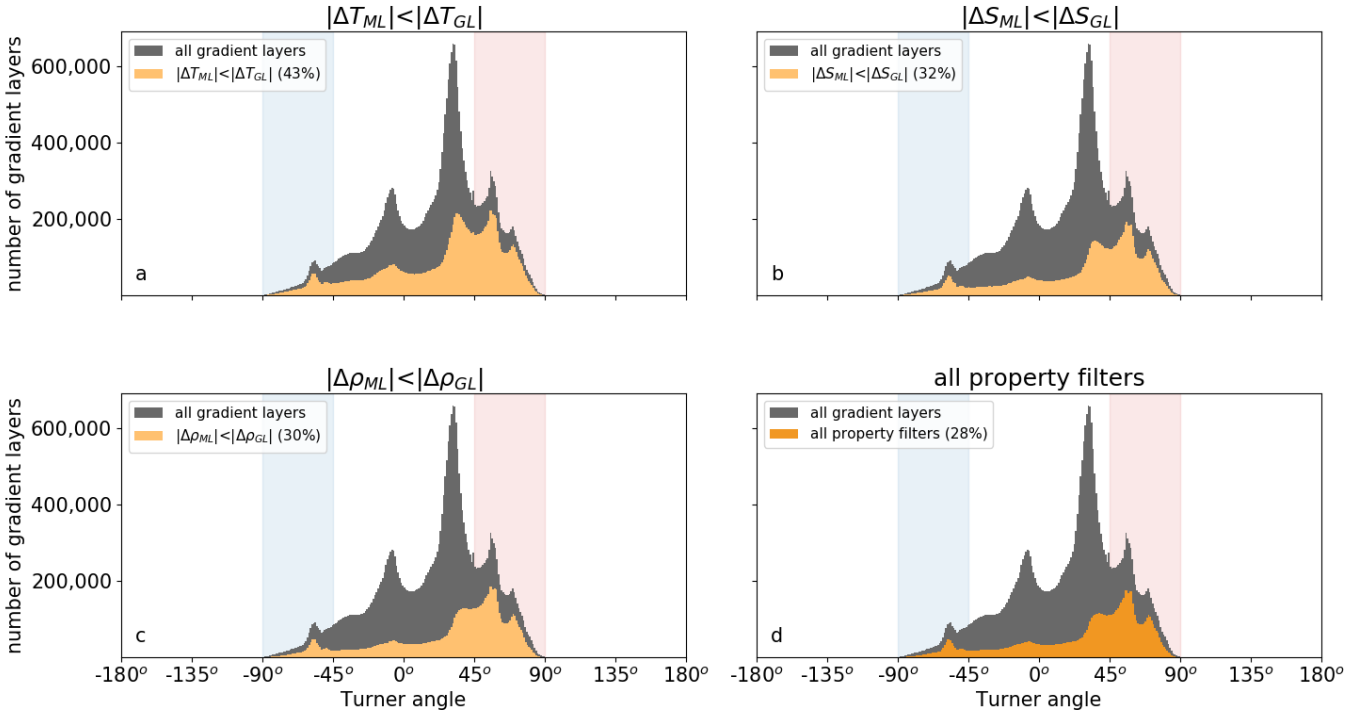

Figure 3. Histogram of the number of detected gradient layers as a function of the Turner angle (Tu) by applying a criteria for (a) temperature, (b) salinity, (c) density and (d) all three properties given in equation 4 (orange shading). Each panel shows the data remaining compared to the raw gradient layer data (grey). Vertical shaded bands correspond to Turner angles in the diffusive-convective (blue) and salt-finger (red) regime.

3.3 Gradient layer: height

The next step in the staircase detection algorithm is to limit the height of the gradient layer (Fig. 2) to ensure that the mixed layers are separated from each other by a relatively thin gradient layer. We require

$$h_{GL} < \min\left(h_{ML,1}, h_{ML,2}\right), \tag{5}$$

i.e. the gradient layer height is smaller than the height of the mixed layers directly above and below the gradient layer. In total, 27 % of the gradient layers that fulfilled the temperature and salinity requirements meet this requirement (Fig. 4a). Note that this part of the algorithm defines the top and bottom of a sequence of a staircase in a profile. However, it appears that this height requirement is not sufficient everywhere. For example, in the Mediterranean Sea thermohaline staircases exist with mixed layers over 100 m and gradient layers of 20 m (Zodiatis and Gasparini, 1996; Radko, 2013). To prevent the false detection of large vertical gradient layers of up to hundreds of meters in profiles with such thick mixed layers, we limit the gradient layer height to $h_{GL,max}$ =30 dbar (Table 1). This only affects the classification of 1 % of the gradient layers (Fig. 4b).

https://doi.org/10.5194/essd-2020-197
Preprint. Discussion started: 11 August 2020

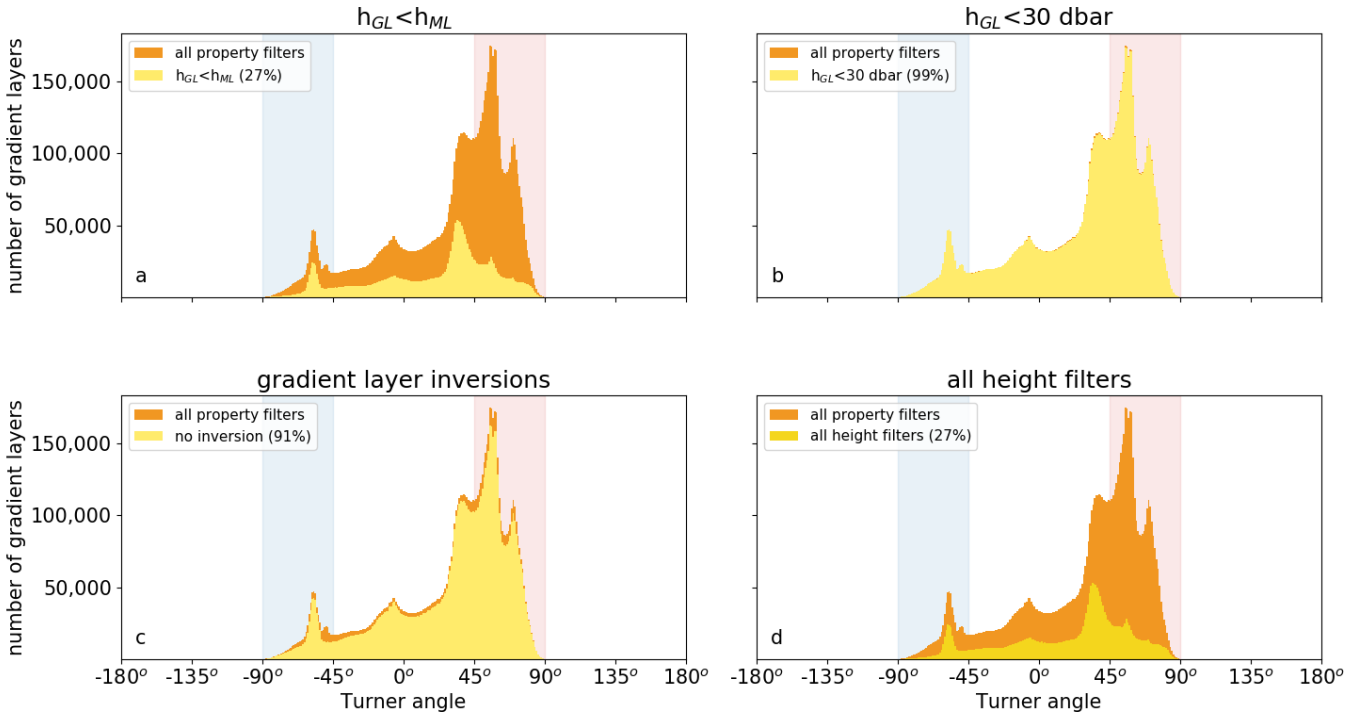

Figure 4. Histogram of the number of detected gradient layers as a function of the Turner angle (Tu) by applying a criteria for (a) height, (b) maximum height, (c) inversions and (d) all three height limitations (yellow shading). Each panel shows the data remaining compared to the gradient layers detected based on the temperature and salinity requirements shown in Fig. 3d (orange shading). Vertical shaded bands correspond to Turner angles in the diffusive-convective (blue) and salt-finger (red) regime.

Furthermore, the tallest observed gradient layers are found in the Mediterranean Sea with heights up to h_{GL} =20 m, where they separate mixed layers of over 100 m . To prevent false detection of large vertical gradient layers of up to hundreds of meters, we limit the gradient layer height to $h_{GL,max}$ =30 dbar (Table 1, Fig. 4b).

To solely detect step-like profiles associated with the presence of thermohaline staircases, the algorithm also removes all gradient layers with temperature or salinity inversions by limiting the number of local minima and maxima of the temperature and salinity allowed in each gradient layer to two (Fig. 4c). The combination of all three gradient layer height requirements is met by 27 % of the gradient layers detected based on the temperature and salinity requirements discussed in the previous section (Fig. 4d).

3.4 Gradient layer: double diffusive regime

After the algorithm has selected all the gradient layers with a step-like structure, the double diffusive regime of each gradient layer is assessed (Fig. 5a). In case both temperature and salinity of the mixed layers above and below the gradient layer increase

https://doi.org/10.5194/essd-2020-197
Preprint. Discussion started: 11 August 2020

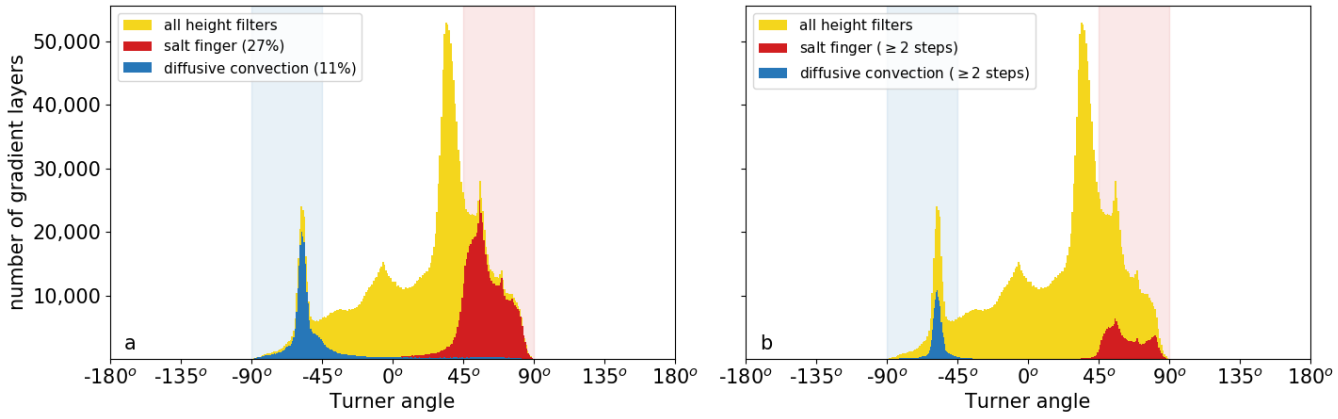

Figure 5. Histogram of the number of detected gradient layers as a function of the Turner angle (Tu) after (a) classification of the double diffusive regime and (b) selection of sequences of the gradient layers. Each panel shows the data remaining compared to the gradient layers detected based gradient layer height requirement shown in Fig. 4d (yellow shading). Vertical shaded bands correspond to Turner angles in the diffusive-convective (blue) and salt-finger (red) regime.

with pressure, the gradient layer is classified as the diffusive-convective regime. If the mixed layer temperature and salinity both decrease with depth, the gradient layer belongs to the salt-finger regime. The algorithm detects more gradient layers in the salt-finger regime (27 %) than in the diffusive-convective regime (11 %, Fig. 5a).

Most gradient layers are found in the salt-finger regime (27%). As expected, most gradient layers with diffusive-convective characteristics have Tu values between $-90° < Tu < -45°$ (blue histogram in Fig. 5a) and most salt-finger gradient layers have Tu values between $45° < Tu < 90°$ (red histogram in Fig. 5a). This implies that these gradient layers properties are consistent with the background stratification.

3.5 Sequences of gradient layers

The final step of the detection algorithm is to only select vertical sequences of at least two gradient layers in the same double diffusive regime separated from each other by one mixed layer (Fig. 5b). In this final step, the algorithm removes also salt-finger gradient layers and diffusive-convective gradient layers outside their favourable Turner angle (compare Fig. 5a and Fig. 5b).

After applying the entire algorithm, we obtain a global dataset consisting of 166,143 gradient layers in the salt-finger regime and 119,619 gradient layers in the diffusive-convective regime. Some examples thermohaline staircases are shown in Figure 6. In line with expectations, staircases in the diffusive-convective regime (Fig. 6a) are mainly detected on the thermocline with temperatures increasing with depth. Thermohaline staircases in the salt-finger regime are detected where the temperature decreases with depth (Fig. 6b). For each thermohaline staircase, characteristics of the gradient layers and mixed layers, such as

https://doi.org/10.5194/essd-2020-197
Preprint. Discussion started: 11 August 2020


Open Access Earth System Science Data Discussions

their temperature, salinity and height, are available in the dataset. An overview of the provided variables is given in Table A1. The detection algorithm is verified by comparing our data to independent observations in three regions in Section 5.

4 Robustness of the detection algorithm

The algorithm requires four input parameters: the moving average window, a threshold for the maximum density gradients of the mixed layers, the maximum density difference of the mixed layers and the maximum height of the gradient layer. In this section, the sensitivity of the algorithm to each input parameter is assessed (Fig. 7).

The moving average window is used by the algorithm to compute the thermal expansion coefficient (α), the haline contraction coefficient (β) and the density ratio (R_ρ). We varied the moving average window between 50 dbar and 350 dbar to assess the sensitivity of the outcomes of this choice (Fig. 7a). We find that the varying moving average window does not result in large variations in detected mixed layers (Fig. 7a).

In contrast to the moving average window, the detection algorithm is sensitive to the value set for the density gradient threshold of the mixed layer (Fig. 7b), which is used to obtain a reference pressure for the sub-surface mixed layers (Section 3.1). Not surprisingly, we detect more (less) gradient layers when we increase (decrease) the allowed threshold density gradient. A small value allows for only the strongest mixed layers to be detected, which are usually referred to as well-defined staircases, while a large density gradient also allows for the detection of rough staircases (e.g., Durante et al., 2019). Although the number of detected gradient layers depends on the value set for this density gradient, the detected gradient layers remain confined to the two double-diffusive regimes, indicating a robust outcome of the algorithm for the choice of this input parameter.

Similar to the variations of the maximum density gradient, the variation of the maximum density difference allowed within the mixed layer results in a different number of detected gradient layers (Fig. 7c). The number of detected mixed layers increases when we decrease the maximum density difference allowed within the mixed layer. This effect is mostly visible in the diffusive-convective regime, as we obtained a decrease of 54 % of detected gradient layers in the diffusive-convective regime compared an decrease of 31 % of detected gradient layers in the salt-finger regime in case we doubled the density difference in the mixed layer ($\Delta\sigma_{1,max} = 10 \times 10^{-3}$ kg m^{-3}). This difference between the regimes is due to relatively small gradient layer variations in the diffusive-convective regime compared to the salt-finger regime (Radko, 2013) and can be explained as follows: When a too large density difference is applied, the relatively small density gradients in the gradient layers of the diffusive-convective regime are detected as mixed layers by the algorithm. Consequently, multiple mixed layers can be identified as a single mixed layer. However, if the applied density difference is too small, this could result in the detection of multiple mixed layers per staircase step.

The last input parameter of the detection algorithm concerns the gradient layer height (Fig. 7d). As expected from Fig. 4b, variations of this input parameter do not result in large differences in the number of detected gradient layers. If we omit this input parameter by setting it to infinity, we obtain a total increase of detected gradient layers of 17 %.

Overall, the detection algorithm gives robust results as it predominantly detects gradient layers within the double-diffusive regime (Fig. 7). In line with expectations, the detection algorithm is most sensitive to the threshold value for the maximum

https://doi.org/10.5194/essd-2020-197
Preprint. Discussion started: 11 August 2020

Open Access Earth System Science Data Discussions

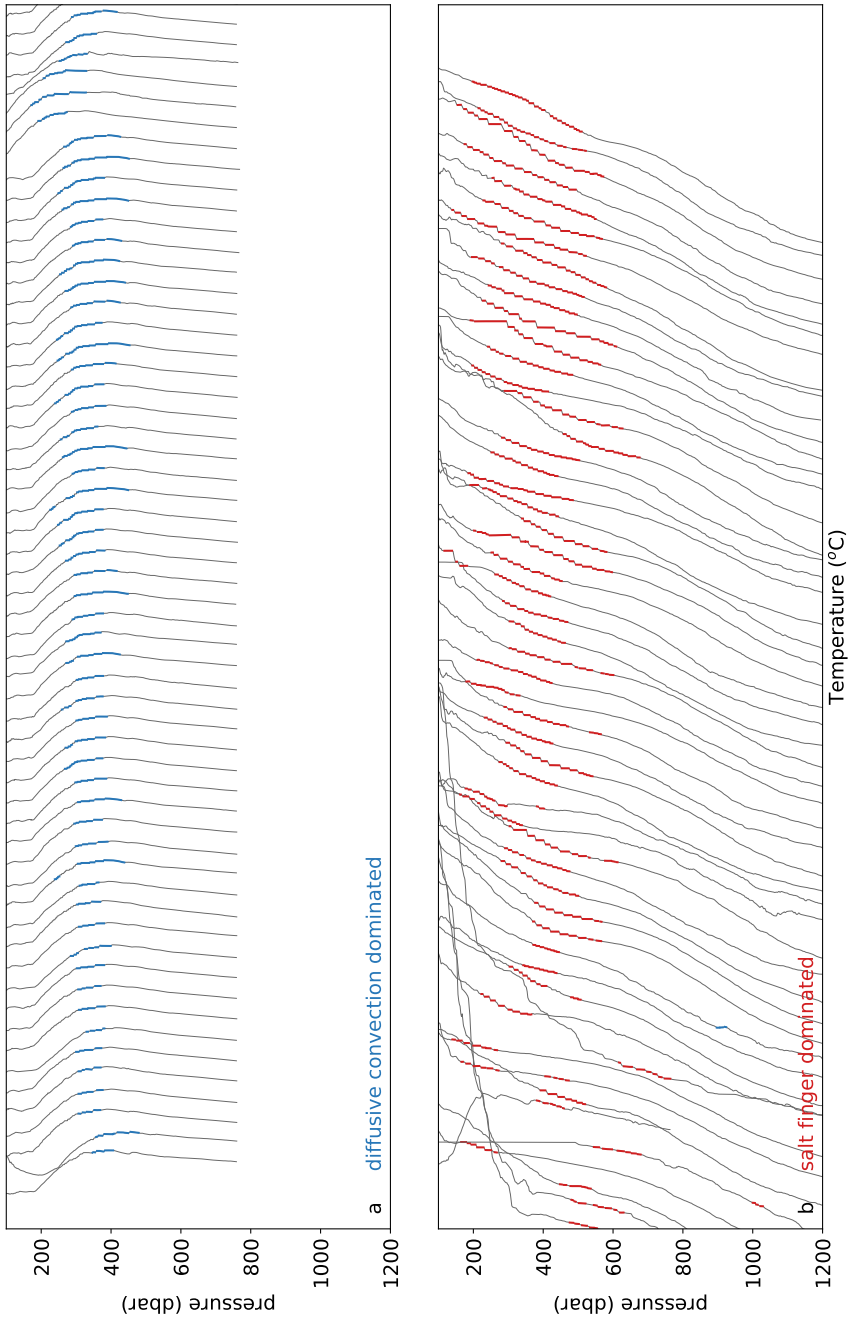

Figure 6. Example temperature profiles selected by the staircase detection algorithm. They are ordered left-right by the number of steps detected. Top panel shows examples of increasing steps of diffusive convection, bottom panel shows examples of the salt-finger regime.

https://doi.org/10.5194/essd-2020-197
Preprint. Discussion started: 11 August 2020

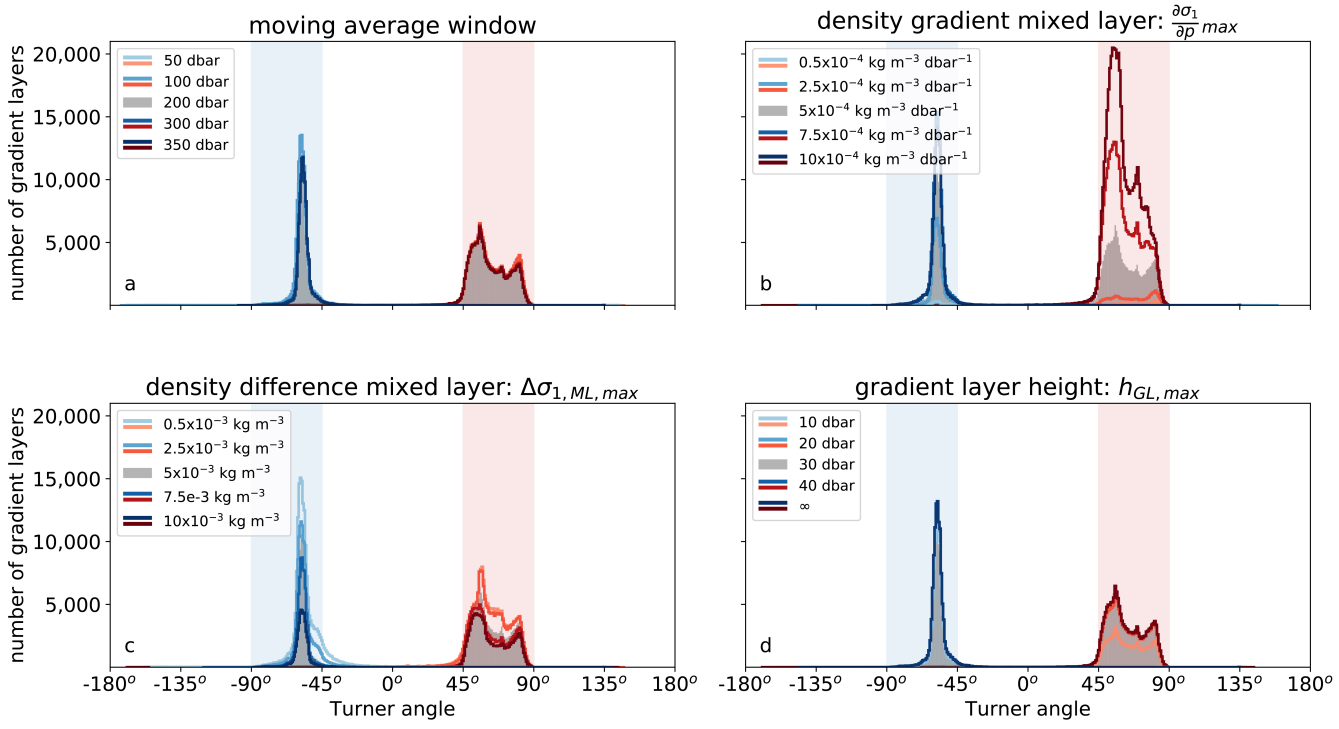

Figure 7. Number of detected gradient layers obtained with the detection algorithm for different input parameters. Each subpanel shows the sensitivity of the detection algorithm to one input parameter: (a) moving average window, (b) density gradient of the mixed layer, (c) density difference within the mixed layer and (d) the maximum height of the gradient layer. In each panel, the grey histogram corresponds to the default parameters listed in Table 1. The colored lines correspond to the varying parameter (see legend). Shaded regions indicate Turner angles in the diffusive-convective (blue) and salt-finger (red) regime.

density gradient in the mixed layer and the density variations within the mixed layers. The four input variables allow for optimalization of the detection algorithm based on the regime and characteristics of the staircases.

5 Regional verification

The characteristics of thermohaline staircases obtained with the detection algorithm are compared to those obtained from previous observational studies for three major staircase regions: the Canada Basin in the Arctic Ocean, the Mediterranean Sea, and the C-SALT region in the tropical Atlantic Ocean. An overview is given in Tables 2-4.

In the Canada Basin (135°W-145°W, 75°N-80°N), the algorithm detects thermohaline staircases in the diffusive-convective regime in 90 % of the profiles (Table 2). Both the occurrence and depth range are comparable to what was reported by Timmermans et al. (2008) and Shibley et al. (2017), who analysed thermohaline staircases from several Ice Tethered Profilers, demonstrating that our detection algorithm indeed detects thermohaline staircases at the right location. Microstructure obser-

https://doi.org/10.5194/essd-2020-197
Preprint. Discussion started: 11 August 2020

Open Access Earth System Science Data Discussions

Table 2. Characteristics of thermohaline staircases in Canada Basin. The region of the global dataset is confined to: 135°W-145°W, 75°N-80°N. The observational techniques indicate if the data was obtained from Argo floats (Argo), Ice Tethered Profilers (ITP), Conductivity Temperature Depth measurements (CTD) or microstructure measurements (MS). The dominant type of thermohaline staircases is indicated by DC (diffusive convection) and SF (salt-finger) with the percentage of occurrence between brackets. Ranges of the obtained variables of the global dataset are indicated by means of the 2.5 and 97.5-percentile.

	technique	type	depth range (dbar)	ΔT_{GL} ($^\circ C$)	ΔS_{GL} (g kg^{-1})	h_{GL} (dbar)
global dataset	ITP+Argo	DC (90 %)	263 - 448	0.007 - 0.1	0.003 - 0.04	2 - 9
Padman and Dillon (1987)	CTD+MS	DC (100 %)	320 - 430	0.004 - 0.013	0.0016 - 0.0049	0.15
Timmermans et al. (2003)	CTD	DC	2400-2900	0.001 - 0.005	0.0035 - 0.0045	2 - 16
Timmermans et al. (2008)	ITP	DC (96 %)	200 - 300	0.04	0.014	
Shibley et al. (2017)	ITP	DC (80 %)		0.04±0.01	0.01 ±0.003	$<$ 1 m

vations suggested that the thermohaline staircases in Canada Basin have gradient layers heights of approximately h_{GL} = 0.15 m. Due to the vertical resolution of the profiles and the design of the algorithm (recall that the mixed layers are separated from each other by removing the upper and lower datapoint of the mixed layer, Section 3.1), it is not capable of detecting very thin gradient layers. Despite these limitations for detection gradient layer heights, the algorithm detects temperature and salinity steps (ΔT_{GL} and ΔS_{GL}, respectively) in the gradients layers that have a magnitude comparable to earlier observations (Padman and Dillon, 1987; Timmermans et al., 2003, 2008; Shibley et al., 2017).

In the Mediterranean Sea, thermohaline staircases are characterized by thick mixed layers that are separated by thick gradient layers of up to 27 m (Zodiatis and Gasparini, 1996). In this region (0°E-15°E, 30°N-43°N), the staircase detection algorithm detected thermohaline staircases with gradient layers up to 21 dbar in 6 % of the profiles, which is comparable to previous observations (Table 3). However, the depth at which the thermohaline staircases occur is underestimated by the detection algorithm, which is due to the limited depth range (mostly 1000 dbar) of the Argo floats in this region. Although the Argo floats, and consequently the detection algorithm, do not cover the full extent of the staircases, the temperature and salinity steps that are found are similar to previous observations. Note that the temperature and salinity steps of the staircases increase with depth (Zodiatis and Gasparini, 1996), which explains why the temperature and salinity steps detected by the algorithm are slightly smaller than those observed in the deeper observations (Zodiatis and Gasparini, 1996; Durante et al., 2019).

In the C-SALT region in the western tropical North Atlantic Ocean (53°W-58°W, 10°N-15°N), the algorithm detected thermohaline staircases in the salt-finger regime in 60 % of the profiles (Table 4). Similar to previous studies (Schmitt et al., 1987, 2005; Fer et al., 2010), the algorithm detected thermohaline staircases on the main thermocline. Again, the gradient layer height is slightly overestimated by the detection algorithm, but the algorithm obtained temperature and salinity steps comparable to previous studies.

https://doi.org/10.5194/essd-2020-197
Preprint. Discussion started: 11 August 2020

Table 3. as Table 2, but for the Mediterranean Sea (0°E-15°E, 30°N-43°N).

	technique	type	depth range (dbar)	ΔT_{GL} ($^{\circ}C$)	ΔS_{GL} (g kg^{-1})	h_{GL} (dbar)
global dataset	ITP+Argo	SF (6 %)	287 - 866	0.0097 - 0.12	0.0017 - 0.031	3 - 21
Zodiatis and Gasparini (1996)	CTD	SF	600 - 2500	0.04 - 0.17	0.01 - 0.04	2 - 27
Bryden et al. (2014)	CTD	SF (32 %)	600 - 1400	0.03 - 0.13	0.009 - 0.03	5 - 16
Buffett et al. (2017)	seismic imaging	SF	550 - 1200			
Durante et al. (2019)	CTD	SF	500 - 2500	approx. 0.15		4 -17

Table 4. as Table 2, but for the western tropical North Atlantic Ocean (53°W-58°W, 10°N-15°N).

	technique	type	depth range (dbar)	ΔT_{GL} ($^{\circ}C$)	ΔS_{GL} (g kg^{-1})	h_{GL} (dbar)
global dataset	ITP + Argo	SF (60 %)	265 - 837	0.019 - 0.97	0.0014 - 0.16	3 - 18
Schmitt et al. (1987)	CTD+MS	SF	180 - 650	0.5 - 0.8	0.1 - 0.2 psu	1 - 10
Schmitt et al. (2005)	CTD+MS	SF	200 - 600	<1		0.5 - 5
Fer et al. (2010)	Seismic imaging	SF	550 - 700			

Overall, the comparison between the outcomes of the detection algorithm with previous studies indicates that the detection algorithm performs well. The small overestimation of the gradient layer height can be attributed to the limited vertical resolution and the limitation imposed by the detection algorithm to avoid detection of false positives. Despite this overestimation, the gradient layers are detected at the correct depths with temperature and salinity steps within the right range. Therefore, we conclude that the detection algorithm is very suitable for the automated detection of thermohaline staircases in large and quickly growing datasets like the Argo float and Ice Tethered Profilers data.

6 Conclusions

In this study, we presented an algorithm to automatically detect thermohaline staircases from Argo float profiles and Ice Tethered Profiles. The design of the detection algorithm is based on the typical vertical structure of the staircases (Fig. 2-4). Note that by formulating the algorithm solely on this vertical structure of the staircases, there is no need to make any assumption about their physical properties beforehand. The Turner angle of the detected staircases indicates that the structures are within the two double diffusive regimes: the salt-finger regime and the diffusive-convective regime (Fig. 5).

https://doi.org/10.5194/essd-2020-197
Preprint. Discussion started: 11 August 2020

A sensitivity analysis to different input parameters showed that the results of the detection algorithm are robust; the detected staircase gradient layers are confined to the double diffusive regimes. Furthermore, a comparison between the detected gradient layer characteristics of thermohaline staircases in three prevailing staircase regions and previous observations, suggested that the detection algorithm accurately captures each double-diffusive regime. Although the gradient layer height was slightly overestimated in two regions, the magnitude of the temperature and salinity steps in the gradient layers was correct, which allows for adequate estimates of the effective diffusivity in thermohaline staircases.

The global dataset resulting from the detection algorithm contains properties and characteristics of both mixed layers and gradient layers. Combined with their locations, this data allows for a statistical analysis of thermohaline staircases on global or regional scales. For example, the global occurrence of thermohaline staircases could give insight in the contribution of double diffusion to the global mechanical energy budget. Moreover, the gradient layer characteristics can be used to validate model and laboratory results on how double diffusive mixing impacts the regional ocean circulation.

7 Code and data availability

Both code and data are available at the 4TU centre for research data (van der Boog et al., 2020). doi: https://doi.org/10.4121/uuid:f6529d31-b285-46ac-990b-5f45839f4e11

Author contributions. CvdB and OK designed the detection scheme. CvdB wrote the paper and was supervised CK, JP and HD who helped shape the analysis and paper.

Competing interests. The authors declare that they have no conflict of interest.

Acknowledgements. The Ice-Tethered Profiler data were collected and made available by the Ice-Tethered Profiler Program (Krishfield et al., 2008; Toole et al., 2011) based at Woods Hole Oceanogaphic Institution (http://www.whoi.edu/itp). The Argo data were collected and made freely available by the International Argo Program and the national programs that contribute to it (http://www.argo.ucsd.edu, http://argo.jcommops.org). The Argo Program is part of the Global Ocean Observing System (Argo, 2000). The work of Carine van der Boog is financed by a Delft Technology Fellowship awarded to Caroline Katsman.

https://doi.org/10.5194/essd-2020-197
Preprint. Discussion started: 11 August 2020

Open Access Earth System Science Data Discussions

Table A1. Metadata of all variables that are saved in the dataset.

variable	unit	description
floatID		float identification number of ITP or Argo float
lat	°E	latitude of observation
lon	°N	longitude of observation
juld	days	julian date of observation
ct	°C	conservative temperature (full profile)
sa	g kg^{-1}	absolute salinity (full profile)
ML_{SF}		mask with mixed layers in the salt-finger regime
ML_{DC}		mask with mixed layers in the diffusive-convective regime
p_{ML}	dbar	average pressure of the mixed layer
h_{ML}	dbar	height of the mixed layer
T_{ML}	°C	average conservative temperature of mixed layer
S_{ML}	g kg^{-1}	average absolute salinity of mixed layer
Tu_{ML}	°	average Turner angle of mixed layer
R_{ML}		average density ratio of the mixed layer
h_{GL}	dbar	height of the gradient layer
Tu_{GL}	°	Turner angle at the center of the gradient layer
R_{GL}		Density ratio at the center of the gradient layer
ΔT_{GL}	°C	conservative temperature difference within the gradient layer
ΔS_{GL}	g kg^{-1}	absolute salinity difference within the gradient layer

References

Argo: Argo float data and metadata from global data assembly centre (Argo GDAC), SEANOE, 2000.

Bebieva, Y. and Timmermans, M. L.: Double-Diffusive Layering in the Canada Basin: An Explanation of Along-Layer Temperature and Salinity Gradients, Journal of Geophysical Research: Oceans, 124, 723–735, https://doi.org/10.1029/2018JC014368, 2019.

Bryden, H. L., Schroeder, K., Sparnocchia, S., Borghini, M., and Vetrano, A.: Thermohaline staircases in the western Mediterranean Sea, Journal of Marine Research, 72, 1–18, 2014.

Buffett, G. G., Krahmann, G., Klaeschen, D., Schroeder, K., Sallares, V., Papenberg, C., Ranero, C. R., and Zitellini, N.: Seismic oceanography in the Tyrrhenian Sea: Thermohaline staircases, eddies, and internal waves, Journal of Geophysical Research: Oceans, 122, 8503–8523, 2017.

Dong, S., Sprintall, J., Gille, S. T., and Talley, L.: Southern Ocean mixed-layer depth from Argo float profiles, Journal of Geophysical Research: Oceans, 113, 2008.

https://doi.org/10.5194/essd-2020-197
Preprint. Discussion started: 11 August 2020

Durante, S., Schroeder, K., Mazzei, L., Pierini, S., Borghini, M., and Sparnocchia, S.: Permanent Thermohaline Staircases in the Tyrrhenian Sea, Geophysical Research Letters, 46, 1562–1570, https://doi.org/10.1029/2018GL081747, 2019.

Fer, I., Nandi, P., Holbrook, W. S., Schmitt, R. W., and Páramo, P.: Seismic imaging of a thermohaline staircase in the western tropical North Atlantic, Ocean Science, 6, 621, 2010.

Garaud, P.: Double-diffusive convection at low Prandtl number, Annual Review of Fluid Mechanics, 50, 275–298, 2018.

Gargett, A. E. and Holloway, G.: Sensitivity of the GFDL ocean model to different diffusivities for heat and salt, Journal of physical oceanography, 22, 1158–1177, 1992.

Holte, J., Talley, L. D., Gilson, J., and Roemmich, D.: An Argo mixed layer climatology and database, Geophysical Research Letters, 44, 5618–5626, 2017.

Kelley, D. E.: Fluxes through diffusive staircases: A new formulation, Journal of Geophysical Research: Oceans, 95, 3365–3371, 1990.

Krishfield, R., Toole, J., Proshutinsky, A., and Timmermans, M.-L.: Automated ice-tethered profilers for seawater observations under pack ice in all seasons, Journal of Atmospheric and Oceanic Technology, 25, 2091–2105, 2008.

McDougall, T. J. and Barker, P. M.: Getting started with TEOS-10 and the Gibbs Seawater (GSW) oceanographic toolbox, SCOR/IAPSO WG, 127, 1–28, 2011.

Merryfield, W. J., Holloway, G., and Gargett, A. E.: A global ocean model with double-diffusive mixing, Journal of Physical Oceanography, 29, 1124–1142, https://doi.org/10.1175/1520-0485(1999)029<1124:AGOMWD>2.0.CO;2, 1999.

Oschlies, A., Dietze, H., and Kähler, P.: Salt-finger driven enhancement of upper ocean nutrient supply, Geophysical research letters, 30, 2003.

Padman, L. and Dillon, T. M.: Vertical heat fluxes through the Beaufort Sea thermohaline staircase, Journal of Geophysical Research: Oceans, 92, 10 799–10 806, 1987.

Polyakov, I. V., Pnyushkov, A. V., Rember, R., Ivanov, V. V., Lenn, Y.-D., Padman, L., and Carmack, E. C.: Mooring-based observations of double-diffusive staircases over the Laptev Sea slope, Journal of physical oceanography, 42, 95–109, 2012.

Radko, T.: Double-Diffusive Convection, Cambridge University Press, Cambridge, https://doi.org/10.1017/CBO9781139034173, http://ebooks.cambridge.org/ref/id/CBO9781139034173, 2013.

Radko, T. and Smith, D. P.: Equilibrium transport in double-diffusive convection, Journal of fluid mechanics, 692, 5–27, 2012.

Ruddick, B.: A practical indicator of the stability of the water column to double-diffusive activity, Deep Sea Research Part A. Oceanographic Research Papers, 30, 1105–1107, 1983.

Schmitt, R. W.: Form of the temperature-salinity relationship in the central water: Evidence for double-diffusive mixing, Journal of Physical Oceanography, 11, 1015–1026, 1981.

Schmitt, R. W., Perkins, H., Boyd, J. D., and Stalcup, M. C.: C-SALT: An investigation of the thermohaline staircase in the western tropical North Atlantic, Deep Sea Research Part A, Oceanographic Research Papers, 34, 1655–1665, https://doi.org/10.1016/0198-0149(87)90014-8, 1987.

Schmitt, R. W., Ledwell, J. R., Montgomery, E. T., Polzin, K. L., and Toole, J. M.: Ocean science: Enhanced diapycnal mixing by salt fingers in the thermocline of the tropical atlantic, Science, 308, 685–688, https://doi.org/10.1126/science.1108678, 2005.

Schroeder, K., Chiggiato, J., Bryden, H., Borghini, M., and Ismail, S. B.: Abrupt climate shift in the Western Mediterranean Sea, Scientific reports, 6, 23 009, 2016.

Shibley, N., Timmermans, M.-L., Carpenter, J., and Toole, J.: Spatial variability of the Arctic Ocean's double-diffusive staircase, Journal of Geophysical Research: Oceans, 122, 980–994, 2017.

https://doi.org/10.5194/essd-2020-197
Preprint. Discussion started: 11 August 2020

Stern, M. E.: The "Salt-Fountain" and Thermohaline Convection, Tellus, 12, 172–175, https://doi.org/10.3402/tellusa.v12i2.9378, https://www.tandfonline.com/doi/full/10.3402/tellusa.v12i2.9378, 1960.

Timmermans, M.-L., Garrett, C., and Carmack, E.: The thermohaline structure and evolution of the deep waters in the Canada Basin, Arctic Ocean, Deep Sea Research Part I: Oceanographic Research Papers, 50, 1305–1321, 2003.

Timmermans, M.-L., Toole, J., Krishfield, R., and Winsor, P.: Ice-Tethered Profiler observations of the double-diffusive staircase in the Canada Basin thermocline, Journal of Geophysical Research: Oceans, 113, 2008.

Toole, J. M., Krishfield, R. A., Timmermans, M.-L., and Proshutinsky, A.: The ice-tethered profiler: Argo of the Arctic, Oceanography, 24, 126–135, 2011.

van der Boog, C. G., Koetsier, J. O., Dijkstra, H. A., Pietrzak, J. D., and Katsman, C. A.: Global dataset of thermohaline staircases obtained from Argo floats and Ice Tethered Profiles, https://doi.org/10.4121/uuid:f6529d31-b285-46ac-990b-5f45839f4e11, https://data.4tu.nl, 2020.

Zodiatis, G. and Gasparini, G. P.: Thermohaline staircase formations in the Tyrrhenian Sea, Deep Sea Research Part I: Oceanographic Research Papers, 43, 655–678, 1996.